# Supporting Information

**Perovskite Quantum Dots Integrated with Vertically Aligned Graphene Toward Ambipolar Multifunctional Photodetectors**

Xiaoqiang Feng[1], Zhengyi He[1],Wei Zhu[1], Menghan Zhao[1], Zhiduo Liu[2], Siwei Yang[3], Shiwei Tang[1], Qinglei Guo[4,6,*], Zhiwen Jin[5,*], Da Chen[1], Guqiao Ding[1,3] and Gang Wang[1,*]

[1]Department of Microelectronic Science and Engineering, School of Physical Science and Technology, Ningbo University, Ningbo 315211, P. R. China.

[2]State Key Laboratory of Integrated Optoelectronics, Institute of Semiconductors, Chinese Academy of Sciences, Beijing 100083, P. R. China.

[3]State Key Laboratory of Functional Materials for Informatics, Shanghai Institute of Microsystem and Information Technology, Chinese Academy of Sciences, Shanghai 200050, P. R. China.

[4]School of Microelectronics, Shandong University, Jinan 250100, P. R. China.

[5]School of Physical Science and Technology & Key Laboratory for Magnetism and Magnetic Materials (MoE), Lanzhou University, Lanzhou 730000, P. R. China.

[6]State Key Laboratory of ASIC and Systems, Fudan University, Shanghai 200433, P. R. China.

*Correspondence to: qlguo@sdu.edu.cn (Q. Guo); jinzw@lzu.edu.cn (Z. Jin); gangwang@nbu.edu.cn (G. Wang)

## *1. Growth of VAGAs*

A 300-nm thick $SiO_2$/Si substrate (1 × 1 $cm^2$) was placed into a furnace. Next evacuated to almost 3 Pa, a mixture of 1 sccm hydrogen ($H_2$) and 10 sccm argon (Ar) flowed into the quartz tube. Then, heat the furnace to the desired temperature. Subsequent closing the mixture of $H_2$ and Ar flow, 5 sccm methane ($CH_4$) was used to prepare the VAGAs. Finally, the furnace was cooled down to 26 °C. The samples reported in this work were prepared at 550 °C applying a plasma power of 150 W for 40 min unless otherwise stated.

### *1.1 Growth temperature*

As shown in **Fig. S1(a)**, the Raman spectra of VAGAs deposited at different temperatures. Four typical Raman peaks of VAGAs can be seen, the 2D peak at 2689 $cm^{-1}$, D' peak at 1610 $cm^{-1}$, G peak at 1581 $cm^{-1}$ and D peak at 1349 $cm^{-1}$. As shown in **Fig. S1(b)**, the peak intensity ratio of $I_D/I_G$ decreases from 3.8 to 2.6. In contrast, $I_{2D}/I_G$ increases from 0.1 to 0.76 with the growth temperature increases from 400 to 550 °C, which indicates the crystal quality improvement as growth temperature increases.[1] Besides, the height of VAGAs is also controlled by growth temperature, as shown in **Figs. S1(c-f).** The 3D AFM images of VAGAs increased gradually with growth temperature increases can be inferred from atomic force microscopy (AFM) characterization.

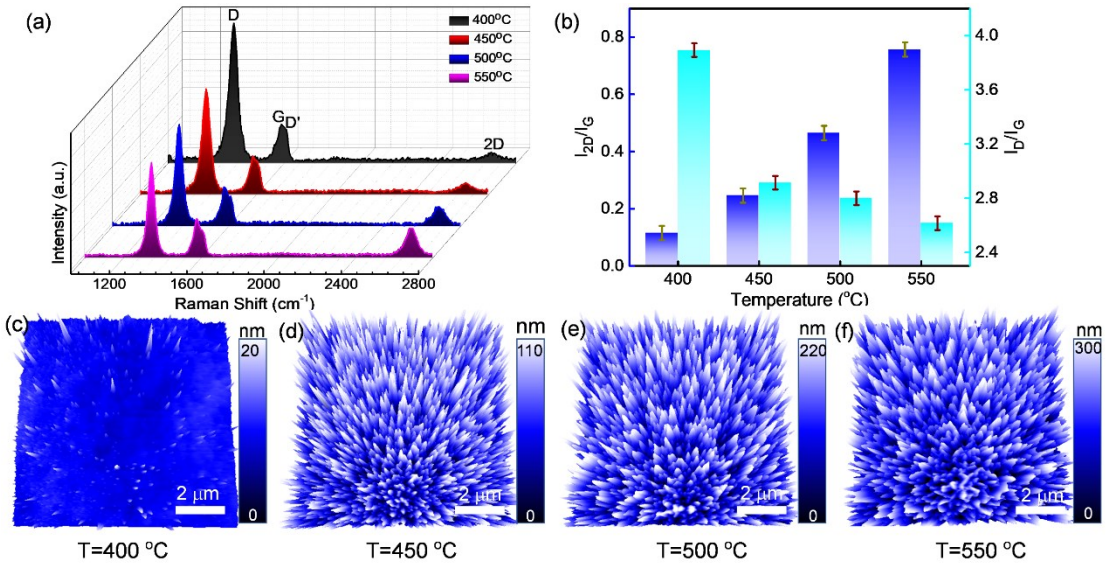

**Fig. S1**. (a) Raman spectra of the VAGAs directly synthesized on $SiO_2$ substrates at the different temperatures from 400 to 550 °C with a growth time of 40 min, plasma power of 150 W. (b) Intensity ratios of $I_D/I_G$ and $I_{2D}/I_G$ as a function of growth temperature. (c-f) 3D AFM images of VAGAs on $SiO_2$ substrates at different temperatures.

### *1.2 Plasma power*

The Raman spectra of VAGAs deposited at various plasma power (75-150 W) are displayed in **Fig. S2(a).** The D-band intensity decreases while 2D-band intensity increases as the plasma power increase from 75 to 150 W. The intensity ratio of $I_D/I_G$ decreases from 2.2 to 1.2 as the plasma power increases, however, the intensity ratio of $I_{2D}/I_G$ increases from 0.25 to 0.85 as shown in **Fig. S2(b).** The height of VAGAs increases with plasma power increases, which can be observed clearly from atomic force microscopy (AFM) characterization shown in **Figs. S2(c-f).**

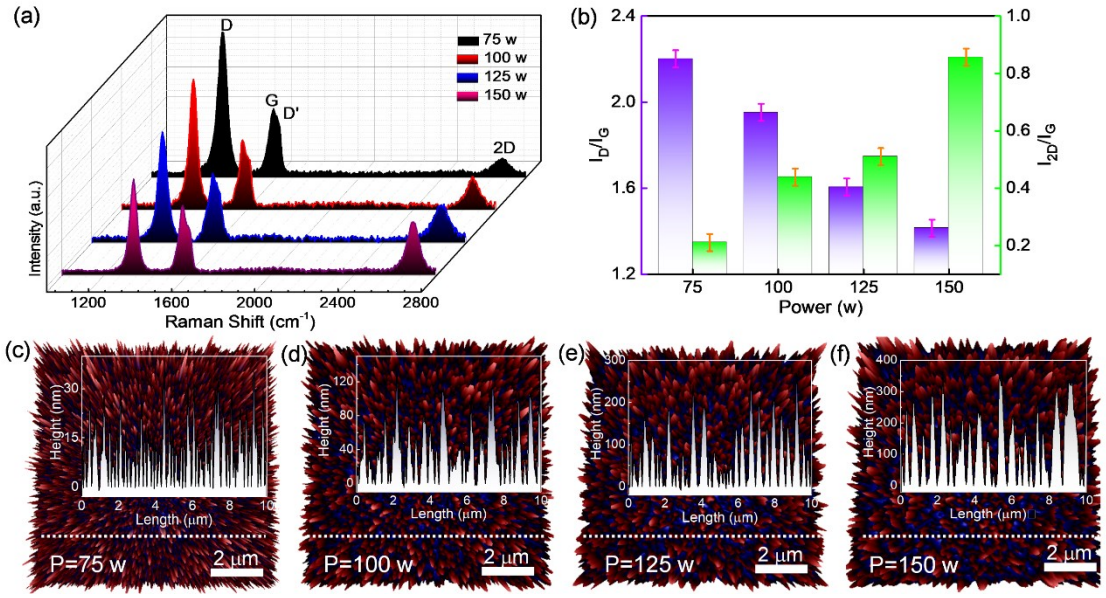


**Fig. S2.** (a) Raman spectra of the VAGAs deposited on $SiO_2$ substrates using different plasma powers with growth temperature of 550 °C and growth time of 40 min. (b) Intensity ratios of $I_D/I_G$ and $I_{2D}/I_G$ as a function of plasma powers. (c-f) AFM images of VAGAs deposited on $SiO_2$ substrates under different plasma powers and the height corresponding to the white spots of the print.

### *1.3 Growth time*

The size of VAGAs increases with growth time increases, which can be observed clearly from the scanning electron microscopy (SEM) morphology shown in **Figs. S3(a-d).** The D-band decreases while 2D-band increases by prolonging growth time, which can be observed in **Fig. S3(e).** The intensity ratio of $I_D/I_G$ decreases as the plasma power increases, however, the intensity ratio of $I_{2D}/I_G$ increases, as shown in **Fig. S3(f).**

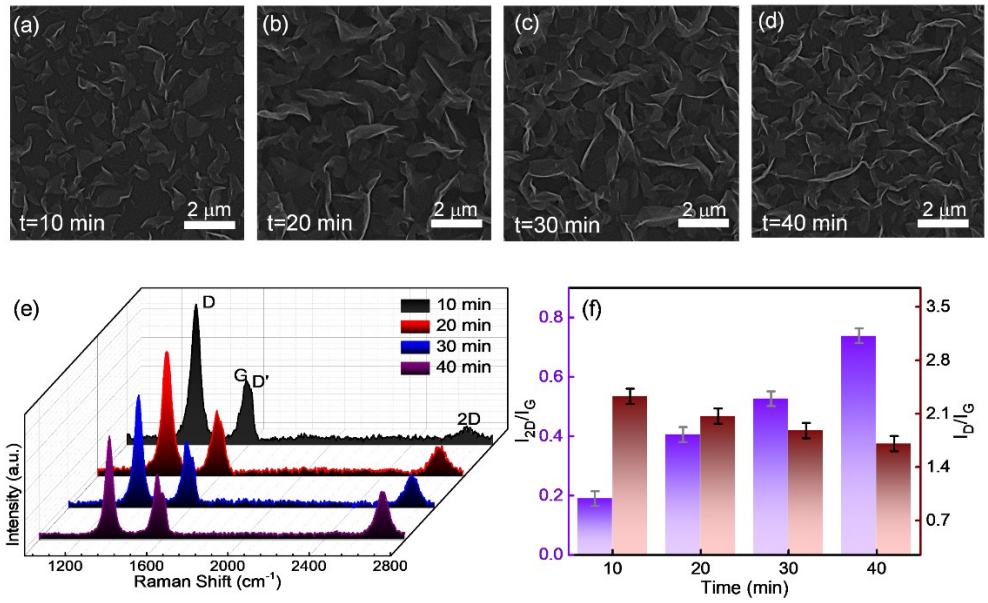


**Fig. S3.** (a-d) SEM images of VAGAs deposited on $SiO_2$ substrates under different time. (e) Raman spectra of the VAGAs deposited on $SiO_2$ substrates with various growth time from 10 to 40 min with deposition temperature at 550 $^oC$ and plasma power for 150 W. (f) The $I_D/I_G$ and $I_{2D}/I_G$ as a function of growth time.

### *2. The characterization of $FAPbI_3$ QDs*

The size-distribution of as-prepared $FAPbI_3$ QDs is revealed by TEM, which demonstrates that the synthesized $FAPbI_3$ QDs is relatively uniform. According to the size-distribution histogram (**Fig. S4**, obtained by counting about 120 particles), the average size of the $FAPbI_3$ QDs is estimated to be 13.5 nm.

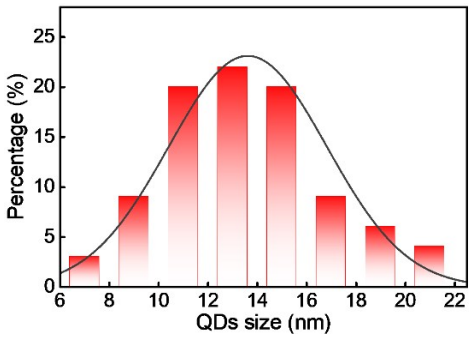


**Fig. S4.** The size distribution histogram of $FAPbI_3$ QDs.

**Fig. S5** exhibits the results of the FT-IR analyses of the $FAPbI_3$ QDs. The 500-3600 $cm^{-1}$ region contains eight superposed bands positioned around 592, 1353, 1466, 1712, 2852, 2923, 3267, 3400 $cm^{-1}$, respectively.[2]

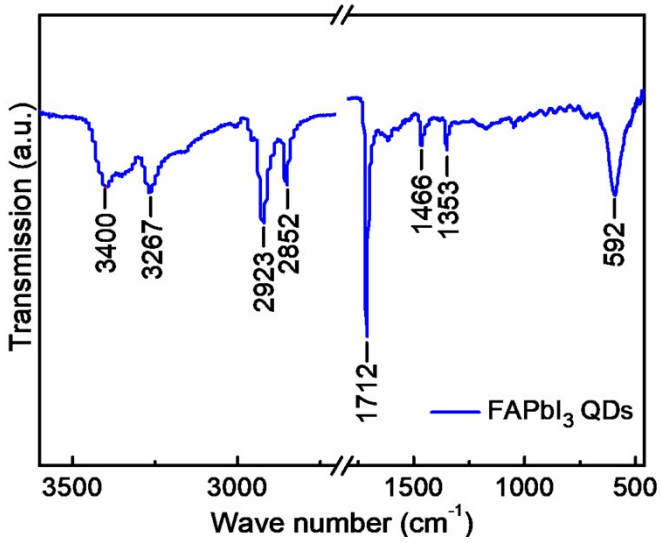


**Fig. S5.** FT-IR spectra of $FAPbI_3$ QDs.

**Fig. S6** displays the contact-mode atomic force microscopy (AFM) morphology of $FAPbI_3$ QDs that are dispersed on the $SiO_2$ substrate with good uniformity. The inset in **Fig. S6** shows the profile of the white dotted line in **Fig. S6,** and the height of $FAPbI_3$ QDs is approximately 1.8 ± 0.2 nm.

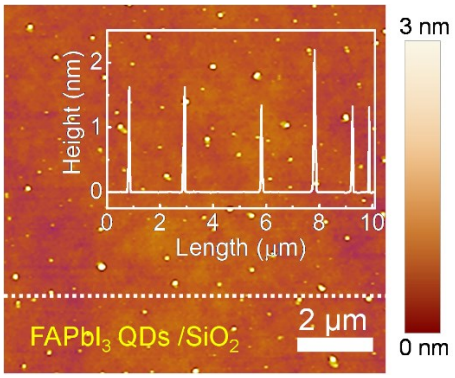


**Fig. S6.** Contact-mode AFM image of $FAPbI_3$ QDs on the $SiO_2$ substrate.

### *3. Characterizations of VAGAs under optimal condition*

### *3.1 The VAGAs with special porosity and high surface to volume ratio building*

**Fig. S7** shows the surface topography of VAGAs and the porosity of VAGAs.

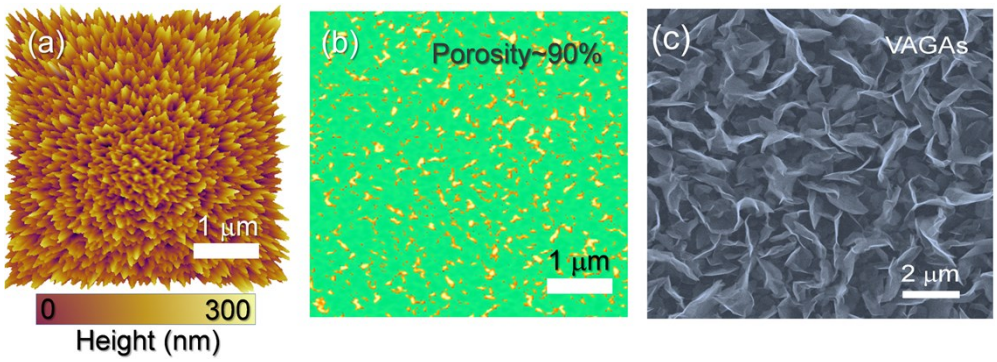


**Fig. S7.** (a) 3D AFM image of the VAGAs on $SiO_2$ substrate. (b) The porosity of AGAs on $SiO_2$ substrate. (c) SEM image of VAGAs/$SiO_2$.

### *3.2 Raman mapping*

The G-band and 2D-band shift Raman mappings of VAGAs/$SiO_2$ are also displayed, as shown in **Figs. S8(a-b).** The uniformity of VAGAs can be inferred. The corresponding G-band and 2D-band displacement histograms of VAGA are shown in **Figs. S8(c-d)**, respectively. By Gauss fitting, it can be known that the G-band position and 2D-band position are at 1581 $cm^{-1}$ and 2689 $cm^{-1}$, respectively.

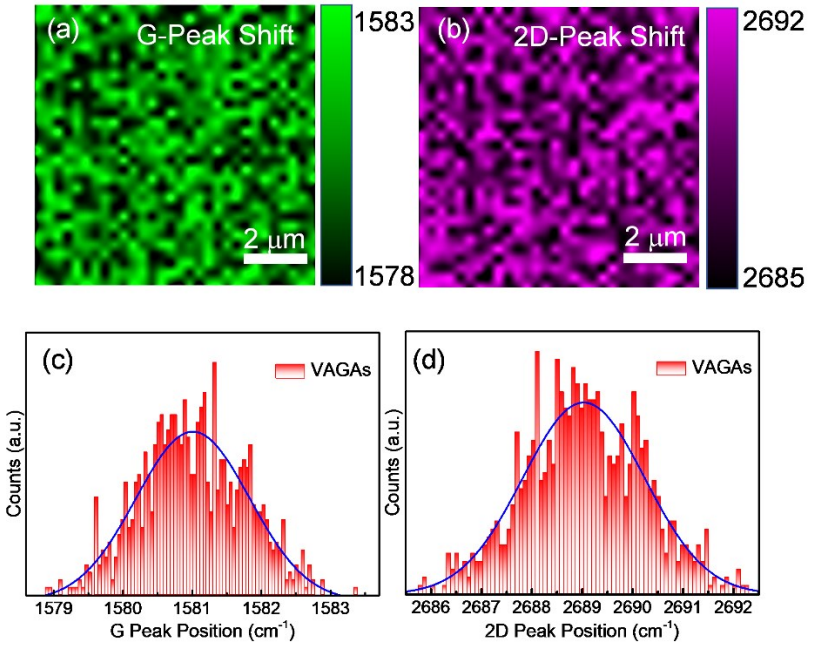


**Fig. S8.** Two-dimensional Raman maps of (a) G-band position and (b) 2D-band position for VAGAs/$SiO_2$. (c) G-band frequency histograms of VAGAs/$SiO_2$. (d) 2D-band frequency histograms of VAGAs/$SiO_2$.

The corresponding G-band and 2D-band shift distribution histograms of $FAPbI_3$ QDs functionalization of VAGAs/$SiO_2$ extracted from Raman mappings are shown in **Fig. S9(a)** and **Fig. S9(b)**. The G-band position is at 1590 $cm^{-1}$ while the 2D-band position is at 2699 $cm^{-1}$.

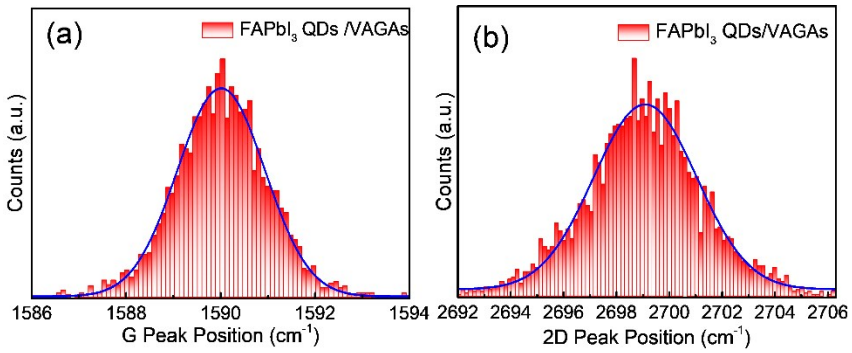


**Fig. S9.** (a) The G-band frequency histograms of $FAPbI_3$ QDs functionalization of VAGAs/$SiO_2$. (b) The 2D-band frequency histograms of $FAPbI_3$ QDs functionalization of VAGAs/$SiO_2$.

***4. Characterizations of $FAPbI_3$ QDs/VAGAs heterojunction***

### *4.1 Survey XPS spectra of $FAPbI_3$ QDs/VAGAs*

The Pb state **Fig. S10(a)** reveals two contributions appearing at 136.91 and 138.44 eV, which are attributed to $Pb^0$ and $Pb^{2+}$, respectively. The N-1s (**Fig. S10(c)**) state is made of two components appearing at a binding energy of 398.51 and 400.72 eV. These two contributions are associated with the nitrogen from the oleylamine used as a capping ligand and the one from the formamidinium.[3,4]

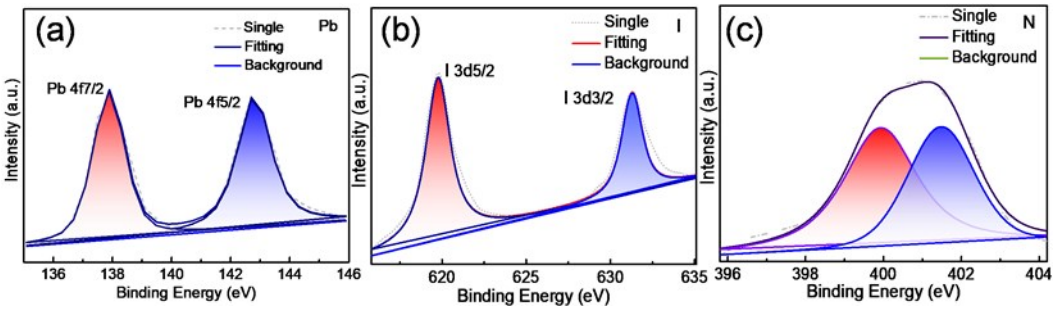


**Fig. S10.** (a) Survey XPS spectra of Pb after functionalization of VAGAs by $FAPbI_3$ QDs. (b) Survey XPS spectra of I after functionalization of VAGAs by $FAPbI_3$ QDs. (c) Survey XPS spectra of N after functionalization of VAGAs by $FAPbI_3$ QDs.

### *4.2 The surface morphology and surface potential of the VAGAs/$SiO_2$ with and without $FAPbI_3$ QDs*

After performing $FAPbI_3$ QDs functionalization, the surface topography of VAGAs/$SiO_2$ does not change, and the curves extracted from **Figs. S11(a-e)** indicate that the heights of the five samples are approximately 300 nm.

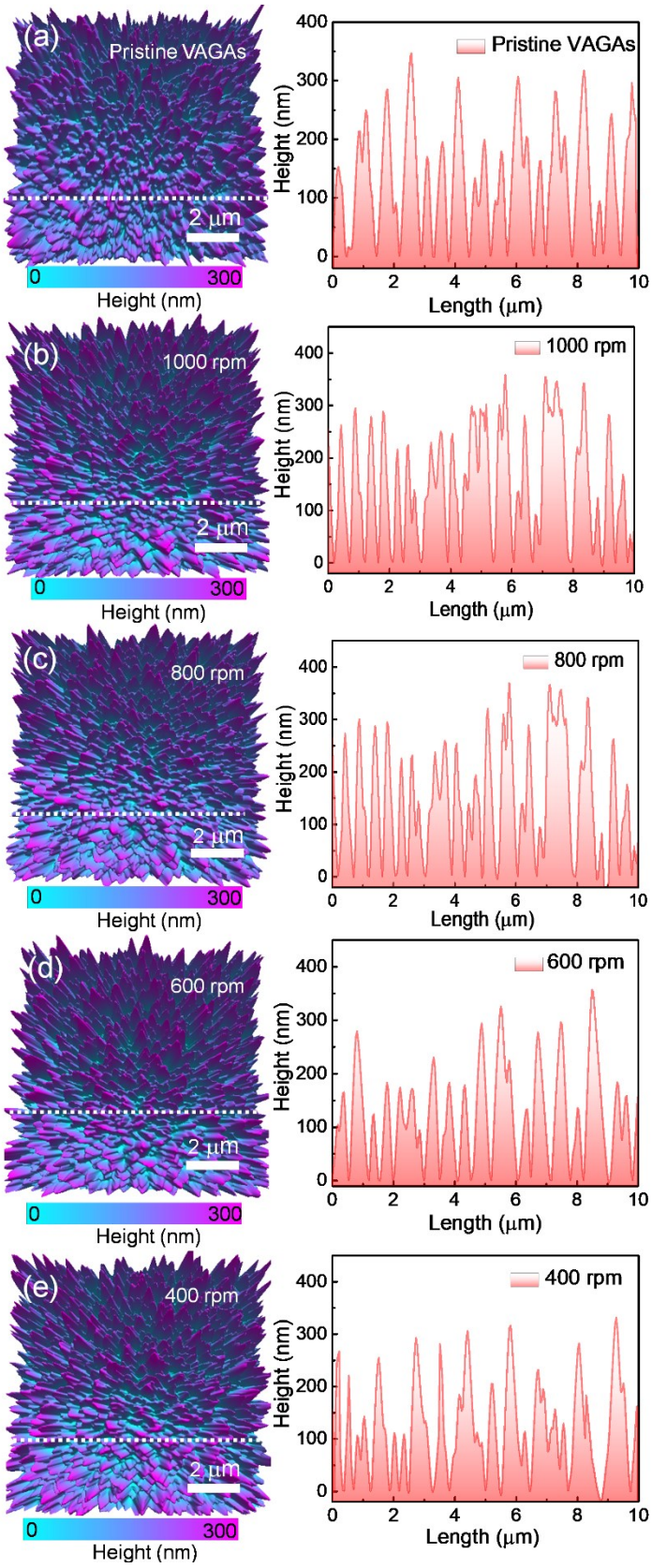


**Fig. S11.** (a) Scanning Kelvin probe microscopy (SKPM) morphology of pristine VAGAs/$SiO_2$ (left) and the height curves of pristine VAGAs/$SiO_2$ (right). (b) SKPM

morphology of VAGAs/$SiO_2$ (left) and the height curves of VAGAs/$SiO_2$ (right) with $FAPbI_3$ QDs spin-coating speed of 1000 rpm. (c) SKPM morphology of VAGAs/$SiO_2$ (left) and the height curves of VAGAs/$SiO_2$ (right) with $FAPbI_3$ QDs spin-coating speed of 800 rpm. (d) SKPM morphology of VAGAs/$SiO_2$ (left) and the height curves of VAGAs/$SiO_2$ (right) with $FAPbI_3$ QDs spin-coating speed of 600 rpm. (e) SKPM morphology of VAGAs/$SiO_2$ (left) and the height curves of VAGAs/$SiO_2$ (right) with $FAPbI_3$ QDs spin-coating speed of 400 rpm.

### *4.3 The surface potential of the VAGAs/$SiO_2$ and histogram statistics of the surface potential distribution.*

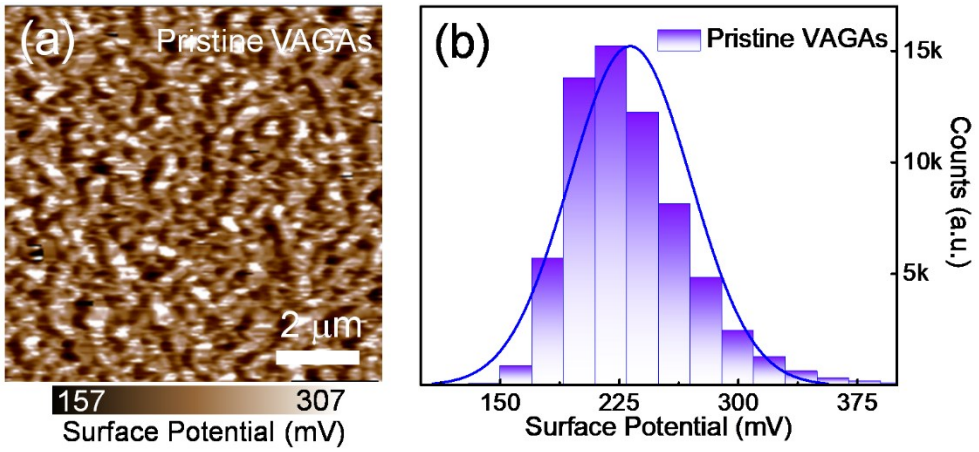


**Fig. S12.** (a) Surface potential distributions of the pristine VAGAs in the dark. (b) Histogram statistics of the surface potential distribution of VAGAs.

### *4.4 The influence of $FAPbI_3$ quantum dots concentration on VAGAs/$SiO_2$ light absorption.*

As shown in the **Fig. S13**, as the spin coating speed increases, the light absorption of VAGAs/$SiO_2$ gradually increases,[5] which explains that $FAPbI_3$ quantum dots can effectively improve the light absorption of VAGAs.

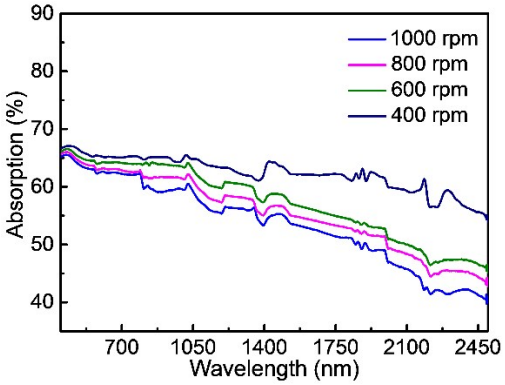


**Fig. S13.** The influence of $FAPbI_3$ quantum dots concentration on VAGAs/$SiO_2$ light absorption.

**References:**

[1] J. Li, Z. Liu, Q. Guo, S. Yang, A. Xu, Z. Wang, G. Wang, Y. Wang, D. Chen and G. Ding, J. Mater. Chem. C, 2019, **7**, 5995-6003.

[2] J. Song, W. Hu, X. F. Wang, G. Chen, W. Tian and T. M, J. Mater. Chem. A, 2016, **4**, 8435-8443.

[3] M. Dufour, J. Qu, C. Greboval, C. Méthivier, E. Lhuillier and S. Ithurria, ACS Nano, 2019, **13**, 5326-5334.

[4] R. C. Shallcross, Y. Zheng, S. S. Saavedra and N. R. Armstrong, J. Am. Chem. Soc., 2017, **139**, 4866-4878.

[5] S. Chandra, S. J. McCormack, M. Kennedy and J. Doran, Solar Energy, 2015, **115**, 552-561.